Langmuir

Article

pubs.acs.org/Langmuir

Templating Gold Surfaces with Function: A Self-Assembled Dendritic Monolayer Methodology Based on Monodisperse Polyester Scaffolds

Kim Öberg,[†] Jarmo Ropponen,[†,‡] Jonathan Kelly,[§] Peter Löwenhielm,[§,∥] Mattias Berglin,*[,⊥] and Michael Malkoch*[,†]

[†]Department of Fibre and Polymer Technology, School of Chemical Engineering, KTH Royal Institute of Technology, SE-100 44 Stockholm, Sweden

[‡]VTT Technical Research Centre of Finland, FI 05201 Rajamäki, Finland

[§]Mölnlycke Health Care AB, Box 130 80, SE 40252 Gothenburg, Sweden

[∥]SP Technical Research Institute of Sweden, Box 857, SE 501 15, Borås, Sweden

[⊥]Cell and Molecular Biology, Interface Biophysics, Göteborg University, SE 40530 Gothenburg, Sweden

Supporting Information

ABSTRACT: The antibiotic resistance developed among several pathogenic bacterial strains has spurred interest in understanding bacterial adhesion down to a molecular level. Consequently, analytical methods that rely on bioactive and multivalent sensor surfaces are sought to detect and suppress infections. To deliver functional sensor surfaces with an optimized degree of molecular packaging, we explore a library of compact and monodisperse dendritic scaffolds based on the nontoxic 2,2-bis(methylol)propionic acid (bis-MPA). A self-assembled dendritic monolayer (SADM) methodology to gold surfaces capitalizes on the design of aqueous soluble dendritic structures that bear sulfur-containing core functionalities. The nature of sulfur (either disulfide or thiol), the size of the dendritic framework (generation 1−3), the distance between the sulfur and the dendritic wedge (4 or 14 Å), and the type of functional end group (hydroxyl or mannose) were key structural elements that were identified to affect the packaging densities assembled on the surfaces. Both surface plasmon resonance (SPR) and resonance-enhanced surface impedance (RESI) experiments revealed rapid formation of homogenously covered SADMs on gold surfaces. The array of dendritic structures enabled the fabrication of functional gold surfaces displaying molecular covering densities of 0.33−2.2 molecules·nm^{-2} and functional availability of 0.95−5.5 groups·nm^{-2}. The cell scavenging ability of these sensor surfaces for *Escherichia coli* MS7fim+ bacteria revealed 2.5 times enhanced recognition for G3-mannosylated surfaces when compared to G3-hydroxylated SADM surfaces. This promising methodology delivers functional gold sensor surfaces and represents a facile route for probing surface interactions between multivalently presented motifs and cells in a controlled surface setting.

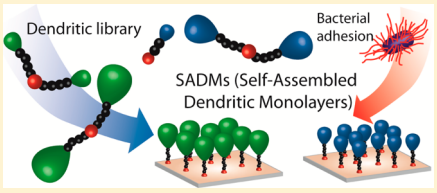

1. INTRODUCTION

The branched structure and dense presentation of functional groups exhibited by dendrimers, along with the very precise control of molecular framework, makes these synthetic macromolecules highly interesting from a biomedical point of view.[1−3] Their versatility has resulted in potential applications such as novel drug delivery vehicles,[4] gel-borne antiviral agents (Starpharma, VivaGel),[5] and tissue engineering of connective tissues.[6] Perhaps one of the most interesting features of dendrimers involves the multivalent representation of ligands enhancing target interactions with biological receptors and cell surfaces.[7,8] The underlying idea of exploiting dendrimers' potential as interaction amplifiers has resulted in increased attention within the field of biosensing and surface recognition applications. In fact, recent reports include dendrimers being used for improving sensitivity of enzyme-linked immunosorbent assays (ELISA),[9] performance enhancement in solar cells,[10] and in dendrimer arrays for functional cell studies.[11,12] However, the common immobilization strategy of dendrimers requires one or several preactivation steps in order to facilitate conjugation to the surface. An alternative and more direct approach for creating dendritic surfaces is to design dendritic scaffolds that include organosulfur groups, for example, disulfides or thiols, which can undergo spontaneous self-assembly to yield monolayers (SAMs) on metal surfaces such as gold and silver.[13−19] Today, it is recognized that dendritic structures provide sufficient surface coverage but do not reach the same monolayer density as commonly observed for linear alkanethiols.[18,20−22] For instance, Gorman et al.[21] described the formation of semipermeable and poorly organized dendritic monolayers from thiol-cored Fréchet-type dendrons of generations 1−3. On the other hand, Zhang et al.[18] reported on the formation of well-ordered nanopatterned stripes using slightly different Fréchet-type dendrons of generations 1−3. It is apparent that the assembly process depends on several factors including type of focal substitution, monomer unit, size

Received: October 18, 2012
Revised: November 29, 2012
Published: December 6, 2012

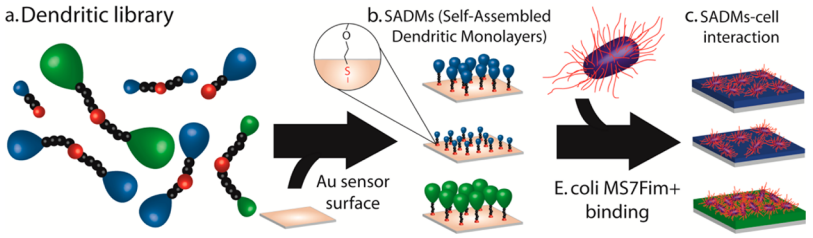

Figure 1. (a) Schematic overview of the dendritic library. (b) Self-assembled dendritic monolayers (SADMs) to provide functional gold sensor surfaces. (c) Cell recognition of SADM sensors by *E. coli* MS7fim+ bacteria.

of dendron and degree of branching, peripheral end-group functionality, temperature, and more.[23,24] Dendritic structures based on the 2,2-bis(methylol)propionic acid (bis-MPA) monomer represent one of the most versatile dendritic families. They can be synthesized in an array of structural variations that have found potential use, such as drug carriers[25] and aqua gels.[26] Their decoration on a variety of surfaces has successfully been reported on gold,[12,13] silicone,[27] and most recently cellulose fibers.[28]

In this paper, we synthesize and investigate the self-assembled dendritic monolayer (SADM) mechanism of a comprehensive sulfur-containing dendritic library based on the bis-MPA dendritic platform (Figure 1). The library included dendrimers and dendrons (macrothiols)[29] of generations 1−3 (G1−G3) and allowed a fundamentally important study of the following structural parameters: (1) impact of thiol (SH) and disulfide (SS) core functionalities, (2) dendron size dependency (branching), (3) effect of the spacer between sulfur core and main dendritic wedge, and (4) peripherial end-group functionality. Surface plasmon resonance (SPR) and resonance-enhanced surface electrochemical impedance (RESI) techniques were employed to monitor the influence of the above parameters. As a final step, uropathogenic *Escherichia coli* MS7fim+ bacteria were exposed to both hydroxyl- and mannose-functionalized surfaces for evaluation of their bacterial scavenging properties.

2. EXPERIMENTAL SECTION

Materials. All chemicals were purchased from Sigma−Aldrich and used as received unless otherwise noted. 2,2-Bis(methylol)propionic acid (bis-MPA) was kindly donated by Perstorp AB.

Nomenclature. The macrothiols described within this work are written with the general formula G#-XX-YY-sp, where G# is the dendron generation; XX is the core functionality (thiol, SH; disulfide, SS; acetylene, acet); YY is the peripheral end-group functionality (hydroxyl, OH; mannose, Man); and sp is added for dendrons with longer spacer between the core and dendrons. For example, G3-SS-OH_{16}-sp corresponds to the generation 3 dendrimer having a disulfide core, 16 terminal hydroxyl groups, and a spacer between the core and dendron wedges.

MALDI-ToF. Matrix-assisted laser desorption ionization time-of-flight mass spectroscopy (MALDI-ToF MS) was conducted on a Bruker UltraFlex MALDI-ToF MS with a Scout-MTP Ion Source (Bruker Daltonics) equipped with a N2-laser (337 nm), a gridless ion source, and a reflector. All spectra were acquired by a linear-positive method with an acceleration of 25 kV. The laser intensity was set to the lowest value possible to acquire high-resolution spectra. The instrument was calibrated with SpheriCal calibrants purchased from Polymer Factory Sweden AB. A tetrahydrofuran (THF) solution of 2-(4′-hydroxybenzeneazo)benzoic acid (HABA; 10 $mg \cdot mL^{-1}$) doped with sodium trifluoroacetate was used as matrix. The obtained spectra were analyzed with FlexAnalysis Bruker Daltonics version 2.2.

^{1}H and ^{13}C NMR. Nuclear magnetic resonance (NMR) experiments were performed on a Bruker Avance 400 MHz instrument. Proton NMR spectra were acquired with a spectral window of 20 ppm, an acquisition time of 4 s, and a relaxation delay of 1 s. ^{13}C NMR spectra were acquired with a spectral window of 240 ppm, an acquisition time of 0.7 s, and a relaxation delay of 2 s.

Flash Chromatography. Flash chromatography was performed by use of 32−64 D 60 Å silica gel from ICN SiliTech (ICN Biomedicals GmbH, Eschwege, Germany).

Surface Plasmon Resonance. The SPR measurements were done on a BIAcore 2000 system (GE Healthcare, Uppsala, Sweden) in a flow cell providing laminar flow, with a flow rate of 5 $\mu L \cdot min^{-1}$. SPR experiments were carried out at 22 °C. The experiments were conducted via the following procedure: (1) A baseline was established with degassed 0.1 M sodium acetate buffer (AcB; pH 5.5) for at least 5 min. (2) Dendron/dendrimer (100 $\mu g \cdot mL^{-1}$) was added to the sample chamber and the binding was observed for 15 min. (3) The sample was washed with pure 0.1 M sodium acetate buffer for at least 5 min. Mass calculations are based on well-established optical models:

$$C_{SPR}\Delta RU = m_{SPR} \quad (1)$$

Equation 1 describes the model used to calculate the SPR adsorbed mass. The constant, C_{SPR}, has been calibrated to be in the range from 6.5×10^{-2} to 1.0×10^{-1} $ng \cdot cm^{-2}$ for a wide range of different organic materials.[30] In this paper the adsorbed mass was calculated with the same value for all dendrons: 6.5×10^{-2} $ng \cdot cm^{-2}$. ΔRU is the measured change in response units (a dimensionless quantity that is proportional to the change in refractive index, Δn, at the interfacial region). It has been shown that the molecular mass of the adsorbing molecule affects the refractive index to some extent. For example, lower values were observed for higher molecular mass proteins.[31] Using the same model for all dendrons is thus not completely correct, but the estimated error is most likely low and is not altering the conclusions presented in this paper. The obtained masses were converted to the number of molecules per square nanometer:

$$D = \frac{\frac{m_{SPR}}{M_n} C_{ch} N_A}{A_{conv}} \quad (2)$$

where D is the density of molecules on the surface, m_{SPR} is the above-described adsorbed mass (grams per square centimeter), M_n is the molecular mass of the adsorbent molecule (grams per mole), C_{ch} is the number of chains/dendrons per molecule (i.e., $C_{ch} = 2$ for disulfide dendrimers and $C_{ch} = 1$ for thiol dendrons), N_A is Avogadro's constant (6.022×10^{23} mol^{-1}), and A_{conv} is an area conversion factor equal to 10^{14}.

Resonance-Enhanced Surface Impedance. By connecting a pair of electrodes in parallel with an external inductance, the electrode pair becomes part of a resonator with a resonance frequency essentially determined by the interface capacitance.[32,33] Shifts in the resonance frequency can then be recorded by mapping the resonance peak, providing a means to resolve capacitance changes of less than 0.2 pF with a time resolution of 0.25 Hz and allowing time-resolved studies of the binding and adsorption events. The capacitance was measured on a dedicated instrument (Layerlab AB, Gothenburg, Sweden) using "Pacman" gold electrodes (electrode area 0.002 cm^2) provided by the instrument manufacturer. RESI measurements were performed under similar conditions as with SPR but with a flow rate of 10 $\mu L \cdot min^{-1}$. At least two measurements per dendron/dendrimer were measured.

dx.doi.org/10.1021/la3041314 | *Langmuir* 2013, 29, 456−465

Sensor Surface Preparation. Gold sensor chips used for both for RESI and SPR experiments were cleaned in a 1:1:5 solution of hydrogen peroxide (25%), ammonia (30%), and Milli-Q water at 85 °C for 10 min and dried in nitrogen gas.

Bacterial Attachment Studies. An *Escherichia coli* strain possessing type 1 fimbriae with specific interaction toward mannose was used in the adhesion studies.[34] Strain MS7pPKL4 (referred to in the text as MS7fim+) contained the *fim* gene cluster on a high-copy-number plasmid. The plasmid configuration was phase-locked on, meaning that all bacteria produce fimbriae.[35] The strain was cultivated at 37 °C in Luria broth agar.[36] All media were supplemented with 50 μg of carbenicillin·mL^{-1} (Duchefa Biochemi, Netherlands). One colony was inoculated in Luria broth[36] and incubated overnight at 37 °C. Growth was monitored spectrophotometrically and cells were harvested in mid-log phase by centrifugation (12100*g*, 10 min), washed three times in phosphate-buffered saline (PBS) and incubated in the same buffer at 21 °C for 24 h. Prior to the experiments, cell suspensions were diluted in the same buffer to 3×10^7 cells·mL^{-1} as determined by light spectroscopy at 600 nm (OD_{600nm} = 0.2). The bacteria solution was added to the parallel flow chamber (Figure S1, Supporting Information) containing SADM sensor surfaces for 30 min under static conditions. Nonadhered and weakly adhered bacteria were removed by rinsing the test surfaces with 300 mL of PBS buffer at a flow rate of 2.5 L·min^{-1}. Attached bacteria were fixed with a solution containing formaldehyde (2.5%) as well as the staining dye Acridine Orange, (0.5 mg·mL^{-1}, Merck, Germany). Before analysis via fluorescence microscopy, the samples were also stained with 4′,6-diamidino-2-phenylindole (DAPI) mounting medium from Vector Laboratories. A minimum of four surfaces per SADM type were analyzed.

Syntheses. The acetylene (acet) cored dendrons G1-acet-OH_2 and G3-acet-OH_8 were synthesized according to earlier described procedures,[37] as was the anhydride of succinic acid monoprop-2-ynyl ester **3**.[38] Azido α-D-mannopyranoside **4** was synthesized by a combination of earlier described procedures described in Supporting Information. Hydroxyl-functional dendrimers (G1−G3)-SS-OH with disulfide core and dendrons (G1−G3)-SH-OH with thiol core of generations 1−3 were synthesized by an earlier reported procedure.[29]

*Methyl 4-Azidobutanoate (**5**).* As shown in Scheme S1A (Supporting Information), methyl 4-chlorobutyrate (25.00 g, 183.0 mmol) was dissolved in 50 mL of dimethyl sulfoxide (DMSO). NaN_3 (35.70 g, 549.1 mmol) was added and the mixture was stirred at 80 °C overnight. The mixture was cooled to room temperature, diluted with 200 mL of diethyl ether, and extracted several times with water. Organic phase was dried with $MgSO_4$ and concentrated to give the product **5** as a colorless oil, yield 25.91 g (98.9%). ^{1}H NMR ($CDCl_3$, 400 MHz, δ) 1.88 (quint, J = 6.97 Hz, 2H, -CH_2), 2.39 (t, J = 7.24 Hz, 2H, -CH_2), 3.32 (t, J = 6.68 Hz, 2H, -CH_2N_3), 3.66 (s, 3H, -CH_3). ^{13}C NMR ($CDCl_3$, 100 MHz, δ) 24.13 (-CH_2), 30.79 (-CH_2), 50.50 (-CH_2), 50.60 (-CH_3), 173.01 (-CO).

*4-Azidobutanoic Acid (**1**).* As shown in Scheme S1A (Supporting Information), methyl 4-azidobutyrate **5** (31.12 g, 217.4 mmol) was dissolved in 260 mL of 1 M NaOH, and 5 mL of MeOH was added to achieve a clear solution. The mixture was stirred at room temperature for 3.5 h, and methanol was evaporated. This solution was extracted twice with diethyl ether (2 × 50 mL), and the H_2O phase was acidified with concentrated HCl and extracted with diethyl ether (3 × 50 mL). The organic phase was dried with $MgSO_4$ and concentrated to give a yellowish oil, yield 25.34 g (90.3%). ^{1}H NMR ($CDCl_3$, 400 MHz, δ) 1.88 (quint, J = 6.95 Hz, 2H, -CH_2), 2.47 (t, J = 7.23 Hz, 2H, -CH_2), 3.37 (t, J = 6.67 Hz, 2H, -CH_2N_3), 10.6 (br s, 1H, -OH). ^{13}C NMR ($CDCl_3$, 100 MHz, δ) 23.86 (-CH_2), 30.87 (-CH_2), 50.39 (-CH_2), 177.17 (-CO).

*Bis(N$_3$)disulfide Core (**2**).* Bis(2-hydroxyethyl)disulfide (2.00 g, 12.97 mmol), 4-azidobutanoic acid **1** (3.52 g, 27.23 mmol), and 2-(dimethylamino)pyridinium toluenesulfonate (DPTS) (1.53 g, 5.19 mmol) were dissolved in CH_2Cl_2 (40 mL) and cooled to 0 °C. *N*,*N*′-Dicyclohexylcarbodiimide (DCC; 6.96 g, 33.71 mmol) was added and the mixture was stirred for 20 h at room temperature. Formed urea was filtered and solvent was evaporated. The crude product was purified by flash chromatography; elution began with heptane and gradually increased in polarity to heptane/ethyl acetate (80:20) to give product **2** as a colorless oil, yield 4.41 g (90.4%). ^{1}H NMR ($CDCl_3$, 400 MHz, δ) 1.90 (quintet, J = 6.95 Hz, 4H, -$CH_2CH_2CH_2N_3$), 2.42 (t, J = 7.24 Hz, 4H, -$CH_2CH_2CH_2N_3$), 2.91 (t, J = 6.54 Hz, 4H, -SCH_2CH_2O), 3.35 (t, J = 6.66 Hz, 4H, -$CH_2CH_2CH_2N_3$), 4.33 (t, J = 6.54 Hz, 4H, -SCH_2CH_2O). ^{13}C NMR ($CDCl_3$, 100 MHz, δ) 24.10 (-$CH_2CH_2CH_2N_3$), 30.94 (-$CH_2CH_2CH_2N_3$), 37.10 (-SCH_2CH_2O), 50.48 (-$CH_2CH_2CH_2N_3$), 62.25 (-SCH_2CH_2O), 172.36 (CO).

G1-SS-OH$_4$-sp. To 5 mL of THF/H_2O (4:1) solution containing G1-acet-OH_2 (0.37 g, 2.17 mmol) and bis(N_3)disulfide core **2** (0.45 g, 1.20 mmol) were added sodium ascorbate (85.0 mg, 0.43 mmol) and $CuSO_4$ (34.0 mg, 0.22 mmol). The reaction mixture was then allowed to stir for 12 h at 40 °C. Solvents were evaporated and the crude product was purified by flash chromatography; elution began with ethyl acetate and gradually increased in polarity to MeOH/ EtOAc (10:90) to give the product as colorless oil, yield 0.75 g (95.8%). ^{1}H NMR (MeOD, 400 MHz, δ) 1.15 (s, 6H, −CH_3), 2.21 (quintet, J = 7.02 Hz, 4H, -$CH_2CH_2CH_2N$), 2.40 (t, J = 7.14 Hz, 4H, -$CH_2CH_2CH_2N$), 2.97 (t, J = 6.38 Hz, 4H, -SCH_2CH_2O), 3.63 (d, J = 10.88 Hz, 4H, -CH_2OH), 3.72 (d, J = 10.88 Hz, 4H, -CH_2OH), 4.33 (t, J = 6.38 Hz, 4H, -SCH_2CH_2O), 4.49 (t, J = 6.93 Hz, 4H, -$CH_2CH_2CH_2N$), 5.24 (s, 4H, -CCH_2O), 8.02 (s, 2H, -NC*H*C). ^{13}C NMR (MeOD, 100 MHz, δ) 17.33 (-CH_3), 26.44 (-$CH_2CH_2CH_2N$), 31.57 (-$CH_2CH_2CH_2N$), 38.05 (-SCH_2CH_2O), 50.50 (-*C*), 51.68 (-$CH_2CH_2CH_2N$), 58.51 (-CCH_2O), 63.54 (-SCH_2CH_2O), 65.82 (-CH_2OH), 125.73 (-*C*), 144.25 (-CH), 173.77 (CO), 176.19 (G1-CO). MALDI-ToF MS calcd for $C_{29}H_{46}N_6O_{11}S_2$, 718.84; found, 743.08 (M + Na).

G3-SS-OH$_{16}$-sp. To 5 mL of THF/H_2O (4:1) solution containing G3-acet-OH_8 (300 mg, 345 μmol) and bis(N_3)disulfide core **2** (71.5 mg, 190 μmol) were added sodium ascorbate (13.7 mg, 69.1 μmol) and $CuSO_4$ (5.5 mg, 34.5 μmol). The reaction mixture was then allowed to stir for 12 h at 40 °C. Solvents were evaporated and the crude product was purified by flash chromatography; elution began with ethyl acetate and gradually increased in polarity to MeOH/EtOAc (20:80) to give the product as white powder, yield 322 mg (88.5%). ^{1}H NMR (MeOD, 400 MHz, δ) 1.15 (s. 24H, G3-CH_3), 1.24 (s. 12H, G2-CH_3), 1.30 (s. 6H, G1-CH_3), 2.23 (quintet, J = 7.03 Hz, 4H, -$CH_2CH_2CH_2N$), 2.42 (t, J = 7.14 Hz, 4H, -$CH_2CH_2CH_2N$), 2.98 (t, J = 6.38 Hz, 4H, -SCH_2CH_2O), 3.59−3.69 (m, 32H, -CH_2OH), 4.19−4.31 (m, 24H, -G1-CH_2 + G2-CH_2), 4.34 (t, J = 6.38 Hz, 4H, -SCH_2CH_2O), 4.51 (t, J = 6.92 Hz, 4H, -$CH_2CH_2CH_2N$), 5.29 (s, 4H, -CCH_2O), 8.10 (s, 2H, -NC*H*C). ^{13}C NMR (MeOD, 100 MHz, δ) 17.33 (G3-CH_3), 18.04 (G1-CH_3), 18.19 (G2-CH_3), 26.45 (-$CH_2CH_2CH_2N$), 31.62 (-$CH_2CH_2CH_2N$), 38.04 (-SCH_2CH_2O), 47.87 (G2-*C*), 47.92 (G1-*C*), 50.58 (-$CH_2CH_2CH_2N$), 51.76 (G3-*C*), 59.09 (-CCH_2O), 63.57 (-SCH_2CH_2O), 65.82 (G3-CH_2OH), 66.12 (G2-CH_2), 67.23 (G1-CH_2), 126.52 (-*C*), 143.52 (-CH), 172.99 (CO), 173.68 (G2-CO), 173.82 (G1-CO), 175.91 (G3-CO). MALDI-ToF MS calcd for $C_{88}H_{140}N_6O_{48}S_2$, 2114.19; found, 2137.11 (M + Na).

G1-SS-acet$_4$-sp. G1-SS-OH_4-sp (0.370 g, 0.513 mmol) and dimethylaminopyridine (DMAP; 0.050 g, 0.411 mmol) were dissolved in pyridine (0.812 g, 10.3 mmol), followed by addition of 30 mL of CH_2Cl_2. The anhydride of succinic acid monoprop-2-ynyl ester **3** (0.785 g, 2.67 mmol) was added slowly. The solution was stirred at room temperature overnight. The reaction was quenched with 5 mL of water under vigorous stirring, followed by dilution with 500 mL of CH_2Cl_2, and the solution was extracted with 10% $NaHSO_4$ (3 × 100 mL), 10% $NaCO_3$ (3 × 100 mL), and brine (50 mL). The organic phase was dried with $MgSO_4$, filtered, and concentrated. The crude product was purified by flash chromatography on silica; elution began with heptane and gradually increased in polarity to ethyl acetate/heptane (60:40) to give G1-SS-acet$_4$-sp, yield 0.605 g (92.5%). ^{1}H NMR ($CDCl_3$, 400 MHz, δ) 1.17 (s, 6H, -CH_3), 2.19 (quintet, J = 6.93 Hz, 4H, -$COCH_2CH_2CH_2N$), 2.34 (t, J = 7.06 Hz, 4H, -$COCH_2CH_2CH_2N$), 2.48 (t, J = 2.44 Hz, 4H, -CH_2CCH), 2.54−2.60 (m, 16H, -$COCH_2CH_2CO$-), 2.87 (t, J = 6.44 Hz, 4H, -SCH_2CH_2O-), 4.17 (ABq, J = 11.03, 7.36 Hz, 8H, -CCH_2O), 4.29 (t, J = 6.50 Hz, 4H,

dx.doi.org/10.1021/la3041314 | *Langmuir* 2013, 29, 456−465

Scheme 1. Assembly of Macrothiol Library[a]

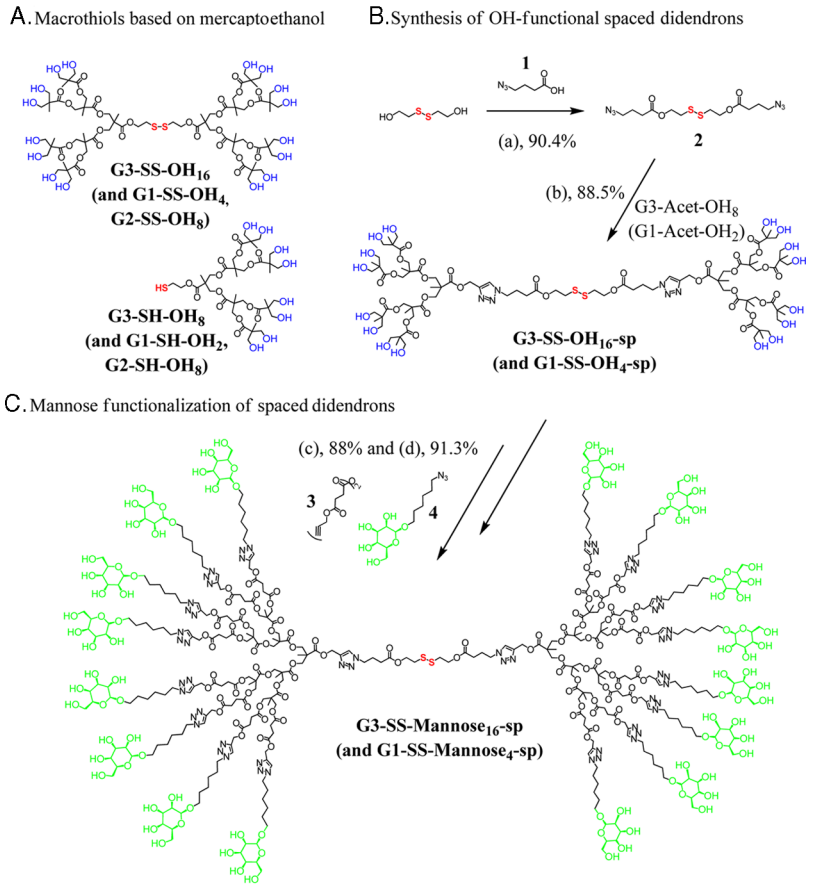

[a](a) **1**, DPTS, DCC, DCM; (b) G3-Acet-OH_8, NaAsc, $CuSO_4$, THF/H_2O; (c) **3**, pyridine, DMAP, DCM; (d) **4**, NaAsc, $CuSO_4$, THF/H_2O.

-SCH_2CH_2O-), 4.40 (t, J = 6.90 Hz, 4H, -$COCH_2CH_2CH_2N$), 4.63 (d, J = 2.44 Hz, 8H, -CH_2CCH), 5.20 (s, 4H, -CCH_2OOCC), 7.65 (s, 2H, -NC*H*C). ^{13}C NMR ($CDCl_3$, 100 MHz, δ) 17.65 (-CH_3), 25.28 (-CH_2), 28.65 (-CH_2), 28.70 (-CH_2), 30.53 (-CH_2), 36.99 (-CH_2), 46.27 (-C), 49.19 (-CH_2), 52.19 (-CH_2), 58.37 (-CH_2), 62.33 (-CH_2), 65.38 (-CH_2), 75.17 (-CH), 77.51 (-C), 124.06 (-CH), 142.36 (-C), 171.31 (CO), 171.34 (CO), 171.96 (CO), 172.41 (CO). MALDI-ToF MS calcd for $C_{56}H_{68}N_6O_{24}S_2$, 1272.32; found, 1295.38 (M + Na).

G3-SS-acet$_{16}$-sp. G3-SS-OH_{16}-sp (115 mg, 54.4 μmol) and DMAP (21.3 mg, 17.4 μmol) were dissolved in pyridine (344 mg, 4.25 mmol), followed by addition of 15 mL of CH_2Cl_2. The anhydride of succinic acid monoprop-2-ynyl ester **3** (333 mg, 1.13 mmol) was added slowly. The solution was stirred at room temperature overnight. The reaction was quenched with 5 mL of water under vigorous stirring, followed by dilution with 500 mL of CH_2Cl_2, and the solution was extracted with 10% $NaHSO_4$ (3 × 100 mL), 10% $NaCO_3$ (3 × 100 mL), and brine (50 mL). The organic phase was dried with $MgSO_4$, filtered, and concentrated. The crude product was purified by flash chromatography on silica; elution began with heptane and gradually increased in polarity to ethyl acetate to give G3-SS-acet$_{16}$-sp, yield 206.8 mg (88.0%). ^1H NMR ($CDCl_3$, 400 MHz, δ) 1.19 (s, 12H, -CH_3), 1.21 (s, 24H, -CH_3), 1.25 (s, 6H, -CH_3), 2.23 (quintet, J = 6.97 Hz, 4H, -$COCH_2CH_2CH_2N$), 2.39 (t, J = 7.31 Hz, 4H, -$COCH_2CH_2CH_2N$), 2.50 (t, J = 2.42 Hz, 16H, -CH_2CCH), 2.60−2.67 (m, 64H, -$COCH_2CH_2CO$-), 2.91 (t, J = 6.52 Hz, 4H, -SCH_2CH_2O-), 4.15−4.27 (m, 56H, -CCH_2O), 4.32 (t, J = 6.52 Hz, 4H, -SCH_2CH_2O-), 4.44 (t, J = 6.92 Hz, 4H, -$COCH_2CH_2CH_2N$), 4.67 (d, J = 2.44 Hz, 32H, -CH_2CCH), 5.23 (s, 4H, -CCH_2OOCC), 7.76 (s, 2H, -NC*H*C). ^{13}C NMR ($CDCl_3$, 100 MHz, δ) 17.41 (-CH_3), 17.45 (-CH_3), 17.74 (-CH_3), 25.35 (-CH_2), 28.71 (-CH_2), 30.62 (-CH_2), 36.95 (-CH_2), 46.36 (-C), 46.57 (-C), 46.62 (-C), 49.25 (-CH_2), 52.20 (-CH_2), 58.48 (-CH_2), 62.39 (-CH_2), 65.29 (-CH_2), 66.11 (-CH_2), 75.15 (-CH), 77.56 (-C), 124.39 (-CH), 142.06 (-C), 171.33 (CO), 171.45 (CO), 171.49 (CO), 171.91 (CO), 172.02 (CO). MALDI-ToF MS calcd for $C_{200}H_{236}N_6O_{96}S_2$, 4324.22; found, 4345.54 (M + Na).

G1-SS-Man$_4$-sp. To 10 mL of THF/H_2O (4:1) solution containing azido α-D-mannopyranoside **4** (199 mg, 653 μmol) and G1-SS-acet$_4$-sp (189 mg, 148 μmol) were added sodium ascorbate (23.5 mg, 119 μmol) and $CuSO_4$ (9.5 mg, 59.4 μmol). The reaction mixture was then allowed to stir for 12 h at 40 °C. Product was dialyzed (MW cutoff 1000) in 5% ethylenediaminetetraacetic acid (EDTA) solution and water and finally lyophilized. The product was obtained as a white solid, yield 348 mg (94.1%). ^1H NMR (MeOD, 400 MHz, δ): 1.21 (s, 6H, -CH_3), 1.30−1.47 (m, 16H, -CH_2), 1.54−1.65 (m, 8H, -CH_2), 1.92 (quintet, J = 7.15 Hz, 8H, -CH_2), 2.21 (quintet, J = 6.91 Hz, 4H, -CH_2), 2.40 (t, J = 7.06 Hz, 4H, -CH_2), 2.59 (s, 16H, -CH_2), 2.96 (t, J = 6.28 Hz, 4H, -CH_2), 3.38 − 3.84 (m, 32H, CH_{Man} + $CH_{2,Man}$ + CH_2), 4.20 (s, 8H, G1-CH_2O), 4.31 (t, J = 6.28 Hz, 4H, -CH_2), 4.42 (t, J = 7.00 Hz, 8H, -CH_2), 4.49 (t, J = 6.78 Hz, 4H, -CH_2), 4.73 (s, 4H, CH_α), 5.20 (s, 8H, -CH_2), 5.26 (s, 4H, -CH_2), 8.05 (s, 4H, -CH), 8.09 (s, 2H, -C*H*). ^{13}C NMR (MeOD, 100 MHz, δ) 18.06 (G1-CH_3), 26.49 (-CH_2), 26.76 (-CH_2), 27.26 (-CH_2), 29.76 (-CH_2), 29.80 (-CH_2), 30.35 (-CH_2), 31.20 (-CH_2), 31.61 (-CH_2), 38.10 (-CH_2), 47.67 (-C), 50.58 (-CH_2), 51.43 (-CH_2), 58.66 (-CH_2), 59.05 (-CH_2), 62.96 (-$CH_{2,Man}$), 63.53 (-CH_2), 66.66 (-CH_2), 68.32 (-CH_{Man}), 68.66 (-CH $_{Man}$), 72.23 (-CH_{Man}), 72.67 (-CH $_{Man}$), 74.62 (-CH $_{Man}$), 101.52 (-CH $_{Man}$), 126.06 (-C), 126.17 (-C), 143.52 (-CH), 143.67 (-CH), 173.24 (CO), 173.61 (CO), 173.79 (CO), 173.88 (CO). MALDI-ToF MS calcd for $C_{104}H_{160}N_{18}O_{48}S_2$, 2494.60; found, 2517.71 (M + Na).

G3-SS-Man$_{16}$-sp. To 9 mL of THF/H_2O (8:1) solution containing azido α-D-mannopyranoside **4** (68.4 mg, 224 μmol), and G3-SS-acet$_{16}$-sp (55.0 mg, 12.7 μmol) were added sodium ascorbate (8.1 mg, 40.7 μmol) and $CuSO_4$ (3.2 mg, 20.4 μmol). The reaction mixture was then allowed to stir for 12 h at 40 °C. Product was dialyzed (MW cutoff

dx.doi.org/10.1021/la3041314 | *Langmuir* 2013, 29, 456−465

1000) in 5% EDTA solution and water and finally lyophilized. The product was obtained as a white solid, yield 107 mg (91.3%). ^{1}H NMR (MeOD, 400 MHz, δ) 1.21 (s, 24H, G3-CH_3), 1.23 (s, 12H, G2-CH_3), 1.29 − 1.46 (m, 70H, -CH_2 + G1-CH_3), 1.53−1.61 (m, 32H, -CH_2), 1.91 (quintrt, J = 7.07 Hz, 32H, -CH_2), 2.21 (m, 4H, -CH_2), 2.41 (t, J = 7.10 Hz, 4H, -CH_2), 2.64 (s, 64H, -CH_2), 2.95 (t, J = 6.20 Hz, 4H, -CH_2), 3.37−3.83 (m, 128H, CH_{Man} + C$H_{2,Man}$ + CH_2), 4.21−4.34 (m, 60H, G1-CH_2 + G2-CH_2 + G3-CH_2 + COOCH_2CH_2S), 4.40 (t, J = 7.00 Hz, 32H, -CH_2), 4.50 (t, J = 6.78 Hz, 4H, -CH_2), 4.72 (d, J = 1.45 Hz, 16H, CH_α), 5.19 (s, 32H, -CH_2), 5.28 (s, 4H, -CH_2), 8.02 (s, 16H, -CH), 8.10 (s, 2H, -CH). ^{13}C NMR (MeOD, 100 MHz, δ) 18.30 (-CH_3), 18.38 (-CH_3), 18.45 (-CH_3), 26.94 (-CH_2), 27.46 (-CH_2), 29.88 (-CH_2), 29.99 (-CH_2), 30.06 (-CH_2), 30.27 (-CH_2), 30.53 (-CH_2), 31.04 (-CH_2), 31.41 (-CH_2), 31.90 (-CH_2), 38.28 (-CH_2), 47.93 (-C), 48.16 (-C), 48.51 (-C), 51.58 (-CH_2), 53.31 (-CH_2), 58.84 (-CH_2), 63.11 (-$CH_{2,Man}$), 63.76 (-CH_2), 66.91 (-CH_2), 68.49 (-CH_{Man}), 68.81 (-CH_{Man}), 72.39 (-CH_{Man}), 72.83 (-CH_{Man}), 74.77 (-CH_{Man}), 101.67 (-CH_{Man}), 126.08 (-C), 126.11 (-C), 144.06 (-C), 173.29 (CO), 173.40 (CO), 173.48 (CO), 173.56 (CO), 173.80 (CO), 173.97 (CO). MALDI-ToF MS calcd for $C_{392}H_{604}N_{54}O_{192}S_2$, 9209.37; found, 9248.1 (M + K).

3. RESULTS AND DISCUSSION

In order to fabricate bioactive sensors displaying an optimized number of dendritic chains at the nanometer scale, we sought to explore the self-assembled dendritic monolayer (SADM) methodology of an array of bis-MPA dendritic structures using gold as a model surface. The choice of surface is associated with its common use as sensor surface in a variety of detection instruments, such as QCM (quartz crystal microbalance), SPR, and RESI. On the basis of the commercial availability of bis-MPA structures,[39] coupled with numerous synthetic reports on a large number of structural variations, we herein investigate a library of dendritic scaffolds containing sulfur units ranging from first to third generation (Scheme 1 and Table 1). The comprehensive library covers structural variations to investigate important parameters, such as the nature of sulfur (-SH or -S-S-) and its distance to the dendritic framework, size of the dendritic wedge, and type and number of peripheral functional groups.

Table 1. Theoretical and Measured Molecular Masses for Library of Macrothiols

name	generation	end group	theor M_n + Na (g/mol)	MALDI[b] (M + Na)
G1-SH-OH_2	G1	2× OH	217.24	
G2-SH-OH_4	G2	4× OH	449.47	
G3-SH-OH_8	G3	8× OH	913.93	913.13
G1-SS-OH_4	G1	4× OH	409.47	
G2-SS-OH_8	G2	8× OH	873.93	873.12
G3-SS-OH_{16}	G3	16× OH	1803.05	1803.05
G1-SS-OH_4-sp	G1	4× OH	743.80	743.08
G3-SS-OH_{16}-sp	G3	16× OH	2137.23	2137.11
G1-SS-Man_4-sp	G1	4× Man	2517.59	2517.71
G3-SS-Man_{16}-sp	G3	16× Man	9248.46[c]	9248.1[c]

[b]Low molecular mass compounds could not be determined due to interference from matrix. [c](M + K) instead of (M + Na).

The Dendritic Library. Two sets of water-soluble dendritic frameworks, having sulfur represented either as a thiol [dendron: G(1−3)-SH-OH_n, n = 2, 4, 8] or a disulfide group [dendrimer: G(1−3)-SS-OH_n, n = 4, 8, 16], were constructed via the divergent growth approach (Scheme 1A).[29] The sulfur units in these sets are spaced with a small ethyl linker from the main framework and with an effective distance of 3.9 Å, calculated by use of CambridgeSoft Chem3D Pro. In both cases, the dendritic precursors self-assemble to identical dendrons on the gold surfaces, enabling a direct and accurate comparison of the nature of the represented sulfur group. The third set of dendritic materials, based on a disulfide core, was synthesized to increase the distance between the sulfur unit and the dendritic wedge by 1 nm to 13.9 Å (Scheme 1B). This was accomplished by employing the highly robust and chemoselective copper-catalyzed azide−alkyne cycloaddition (CuAAC) click reaction.[40] The strategy relied on the synthesis of an azide-functional spacer, in this case 4-azidobutanoic acid **1**, that was covalently coupled to bis(2-hydroxyethyl)disulfide through an esterification reaction. After purification, bis(N_3)-disulfide core **2** was obtained in 90% yield. The isolated azide-functional core was efficiently reacted with acetylene-cored bis-MPA dendrons, G1-acet-OH_2 and G3-acet-OH_8, via the CuAAC reaction and in a THF/H_2O solvent mixture. The attach-to-approach yielded first- and third-generation disulfide dendrimers, G1-SS-OH_4-sp and G3-SS−OH_{16}-sp, in 96% and 89% yields, respectively. Figure 2 illustrates the purity of G3-SS-OH_{16}-sp by both ^{1}H NMR and MALDI-ToF. To further demonstrate the potential use of the bis-MPA dendritic platform as biosensors for cell-to-surface recognition, SADM surfaces with multiple carbohydrate ligand representation were successfully accomplished by a facile two-step modification (Scheme 1C). In this case, the peripheral hydroxyl groups of G1-SS-OH_4-sp and G3-SS-OH_{16}-sp were decorated with acetylenes via mild anhydride chemistry[41] followed by selective CuAAC postmodifications with an azide-functional carbohydrate moiety (azido α-D-mannopyranoside **4**). Mannose activation of the dendritic wedges was monitored with NMR and MALDI-ToF, and the isolated products were accomplished in +90% yields for both G1-SS-Man_4-sp and G3-SS-Man_{16}-sp.

Functional SADM Surfaces. *Influence of Dendritic Wedge Size and Type of Sulfur Group.* To assess the SADM mechanism for both thiol- and disulfide-based dendritic wedges, surface plasmon resonance (SPR) was employed. SPR is an optical technique that allows excellent sensitivity down to picogram per square millimeter levels; it may be operated in a variety of solvents and enables in situ high-resolution monitoring of the adsorption process.[42] Figure 3 shows the SPR chart of first- and third-generation dendrons with thiol core (G1-SH-OH_2 and G3-SH-OH_8) and dendrimers with disulfide core (G1-SS-OH_4 and G3-SS-OH_{16}). The adsorptions were measured during 15 min long injections of 100 μM dendron solutions in 0.1 M sodium acetate buffer (pH 5.5). It is apparent that both the size of the dendritic wedge and the nature of the sulfur play important roles in the gold binding profile and the amounts that are successfully attached.

As can be seen in Figure 3, the injection of G1-SH-OH_2 and G1-SS-OH_4 yielded approximately equally dense layers of ca. 70 ng·cm^{-2}. This corresponds to an average of 2 molecules or 4 terminal hydroxyl groups per square nanometer (Table 2 and Figure 4). However, in contrast to linear disulfides and thiols, which commonly exhibit similar binding profiles,[43] branched dendritic molecules reveal two different binding profiles indicating two different modes of adsorption. The adsorption of G1-SH-OH_2 with a free thiol is nearly instantaneous, indicating a very direct binding to the surface, whereas the G1

dx.doi.org/10.1021/la3041314 | Langmuir 2013, 29, 456−465

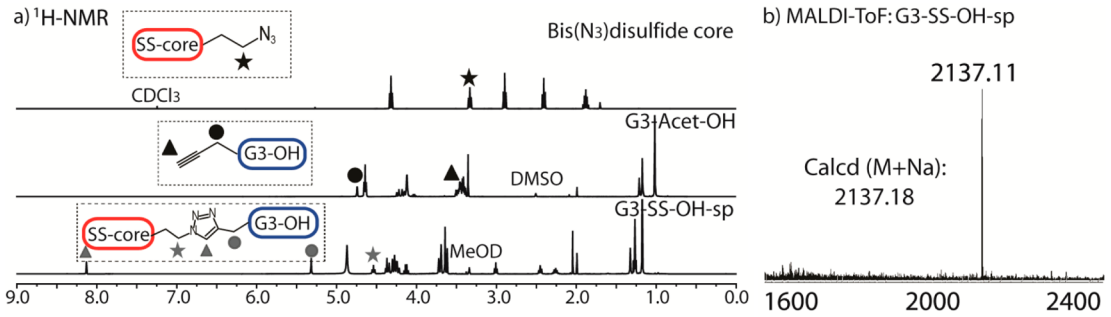

Figure 2. Synthesis of G3-SS-OH_{16}-sp, monitored by (a) ^{1}H NMR and (b) MALDI-ToF MS.

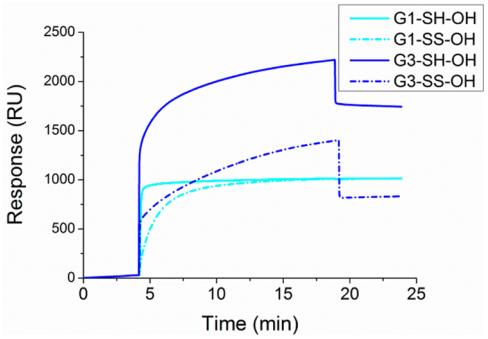

Figure 3. SPR response of G1/G3-SH-OH and G1/G3-SS-OH binding to gold surfaces in sodium acetate buffer (pH 5.5) for a duration of 15 min, followed by a 5 min wash procedure.

Table 2. Hydroxyl-Functional SADMs of Generations G1–G3 with Thiol or Disulfide Cores[a]

name	SPR response (RU)	surface attachment (ng·cm^{-2})	dendron density (molecules·nm^{-2})	funct group density (OH·nm^{-2})
G1-SH-OH_2	1048 ± 115	68.1 ± 7.5	2.1 ± 0.2	4.2 ± 0.5
G1-SS-OH_4	1100 ± 253	71.5 ± 15.2	2.2 ± 0.5	4.5 ± 0.9
G1-SS-OH_4-sp	1363 ± 231	88.6 ± 15.0	1.5 ± 0.3	3.0 ± 0.5
G2-SH-OH_4	1134 ± 228	73.7 ± 14.8	1.0 ± 0.3	4.2 ± 0.8
G2-SS–OH_8	871 ± 37	56.6 ± 2.4	0.8 ± 0.03	3.2 ± 0.1
G3-SH-OH_8	1395 ± 300	90.7 ± 19.5	0.61 ± 0.1	4.9 ± 0.5
G3-SS-OH_{16}	905 ± 83	58.8 ± 5.4	0.40 ± 0.04	3.2 ± 0.3
G3-SS-OH_{16}-sp	1865 ± 369	121.2 ± 24.0	0.69 ± 0.1	5.5 ± 1.1

[a]Measured by SPR in sodium acetate buffer (pH 5.5).

disulfide has a slower packaging profile. This difference may be due to a shielding effect whereby disulfide accessibility is limited by the dendritic G1 substituent. For both G1 surfaces, no physically entrapped molecules could be detected after a 5 min purging cycle supporting permanent and successful attachments. The type of sulfur and the dendritic shielding effect on the amounts bound during the initial phase were even more influenced for the higher-generation dendritic wedges (Table 2). The most dramatic difference in adsorption could be detected between G3-SH-OH_8 and G3-SS-OH_{16} (Figures 3 and 4). A direct comparison between the two SADMs displays ca.

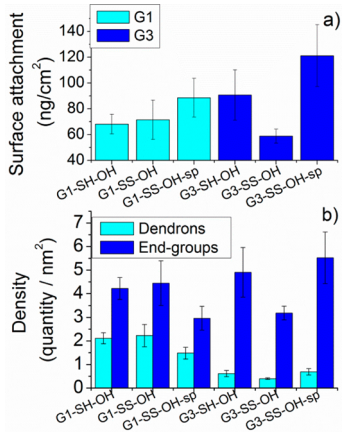

Figure 4. (a) Surface attachment of OH-functional dendrons, generations G1 and G3 with varying core structures, measured by SPR in sodium acetate buffer (pH 5.5). (b) Values converted into number of dendrons and hydroxyl-functional groups (OH).

91 ng·cm^{-2} (0.6 molecule·nm^{-2}) for G3-SH-OH_8 and 59 ng·cm^{-2} (0.4 molecule·nm^{-2}) for G3-SS-OH_{16}. This corresponds to a packaging density increase of 54 wt % for G3-SH-OH_8 when compared to G3-SS-OH_{16}. Interestingly, both G3 scaffolds displayed a drop upon the purging cycle, indicating the presence of low-affinity-binding dendritic wedges (Figure 3). Such mechanisms may arise from nonspecific interactions of the large number of hydroxyl groups present at the periphery of the dendritic scaffolds[13] or the formation of multilayers. Nonetheless, covalently attached SADMs exhibiting hydroxyl functional groups were successfully produced and supported by a constant attachment level, even after 18 h of extensive purging under continuous sodium acetate buffer flow. The above-described behavior for higher-generation dendritic scaffolds is commonly observed for branched alkanethiols and disulfides,[23] where unfavorable intermolecular interactions between the substituting chains of disulfides prohibits close packing. Additionally, the adsorbed masses of the disulfide-based G2-SS-OH_4 (57 ng·cm^{-2}) and G3-SS-OH_8 (59 ng·cm^{-2}) were lower than their corresponding G1-SS-OH (72 ng·cm^{-2}), in spite of the much larger molecular mass (Table 1), indicating a strong inhibition effect of the dendritic wedges on the SADM mechanism.

Effect of Spacer between the Sulfur and Dendritic Wedge. Capitalizing on the impact of both the nature of sulfur groups and size of the dendritic wedges on the functionalization degree of gold surfaces, we sought to determine the binding efficiency of hydroxyl functional dendritic wedges displaying a longer spacer between the sulfur group and the main dendritic wedge.

dx.doi.org/10.1021/la3041314 | Langmuir 2013, 29, 456–465

Both G1-SS-OH_4-sp and G3-SS-OH_{16}-sp with a 13.9 Å long disulfide spacer resulted in increased adsorbed amounts when compared with G1-SS-OH_4 and G3-SS-OH_{16} having a 3.9 Å spacer (Figure 4a). For G1-SS-OH_4-sp, 89 ng·$cm^{-2}$was successfully attached, which exceeded the deposition levels of the short-spacer thiol compounds of ca. 70 ng·cm^{-2}. However, the pure mass deposited does not detail the overall picture of the functionalization degree of the surface due to the substantial difference in molecular mass of the adsorbed compounds (Table 1). Normalizing toward the molecular weight of G1-SS-OH_4-sp revealed a decrease in the number of molecules and hydroxyl groups successfully attached (1.5 molecules·nm^{-2} and 3.0 OH·nm^{-2}). However, in the case of G3-SS-OH_{16}-sp, 121 ng·cm^{-2} was efficiently attached, which corresponds to 0.69 molecule·nm^{-2} and 5.5 OH·nm^{-2}. It is apparent that increased length of the spacer for G3-SS-OH_{16}-sp enabled a ca. 70% denser SADM when compared to G3-SS-OH_{16} with 0.4 molecule·nm^{-2} (Figure 4). Additionally, despite the relatively large size of the dendritic framework coupled with the short assembly time, the resulting functional group density is in the same range as a well-packed layer of linear alkanethiols.[44]

Impact of Cosolvent, End Group, and Number of Injections. The effect of cosolvents and number of injections on SADM mechanism was assessed for the dendritic library containing a spacer as the G3-SS-OH_{16}-sp set displayed the highest binding affinity to gold surfaces. As alcohols are typically used as solvents during the synthesis of bis-MPA dendritic materials, a benign 70% ethanol solution was required to fully solubilize the scaffolds. Interestingly, while the solvent exchange from sodium acetate revealed approximately the same absorption for G1-SS-OH_4-sp, a large change in the adsorption was found for G3-SS-OH_{16}-sp, which was reduced from 121 ng·cm^{-2} in AcB to 57 ng·cm^{-2} in ethanol (Figure 5a and Table 3). The 47% lower mass attachment of G3-SS-OH_{16}-sp corresponds to 0.33 molecule·nm^{-2} and functional group density of 2.6 OH·nm^{-2}. This could be reasoned as an effect of ethanol being a superior solvent for the bis-MPA dendritic scaffolds, resulting in a more extended geometry that occupies a larger surface area upon attachment, hence affecting the binding affinity negatively. To fabricate sensor surfaces with bioactive functionalities while also assessing the influence of end groups on the SADM mechanism, mannose groups were chosen for attachment to the dendritic periphery because they represents a bulky terminal moiety with well-known binding efficacy to cell receptors. A direct comparison between G1-SS-OH_4-sp and G3-SS-OH_{16}-sp and their mannose-functionalized derivatives (G1-SS-Man_4-sp and G3-SS-Man_{16}-sp) (Scheme 1C) was conducted in 70% ethanol. As can be seen in Figure 5a, the largest mass absorption was found for G3-SS-Man_{16}-sp with a value of 127 ng·cm^{-2}. However, after normalization to the molecular weight of the dendritic wedges, the actual number of chains attached to the gold surface is higher for the hydroxyl-functional dendrons (Figure 5b).The large decrease of attached molecules for G3-SS-Man_{16}-sp (0.17 molecule·nm^{-2} or 1.3 mannose·nm^{-2}) is likely an effect of size, since the dendron molecular mass is 4604 g·mol^{-1}, which is over 5 times larger than G3-SS-OH_{16}-sp with dendron mass of 890 g·mol^{-1}. Nevertheless, the number of successfully attached molecules is over 2-fold higher compared to linear 5 kDa thiol-functional poly(ethylene glycol) molecules (PEG-5k-SH) with a binding efficiency of 0.07 molecule·nm^{-2}. In contrast to the SPR technique with absorbed mass detection, RESI reveals the structural integrity by measuring the capacitance of the adlayer.

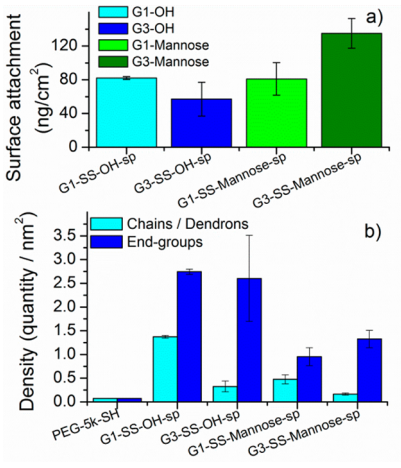

Figure 5. Surface attachment of hydroxyl- and mannose-functional dendrons generation G1 and G3 on Au surface measured by SPR in 70% EtOH. (a) Mass binding efficiency; (b) molecular/end-group density with linear PEG-5k-SH as reference.

The potential presence of cavities in the SADMs will permit easier ion penetration, hence a high capacitance will be recorded as free gold surface will be exposed against the instrument interface. As with SPR, a rapid and stable capacitance was obtained within minutes and maintained even after prolonged washing indicating that no significant rearrangements occur over time (Figure 6). The rather large decrease in mass of the G3 compounds detected with SPR after purging cycles was not observed by a change in capacitance levels with RESI. This further strengthens the hypothesis that the dendritic wedges are densely attached and form SADMs on injection, and further attachment of weak and unspecific assembled multilayers is formed in a secondary process. The detected capacitance for the four SADMs ranged between 4.76 and 7.35 μF·cm^{-2}. These values reveals that SADMs are densely packed and in the range of well-insulated hydrophobic SAM layers, which are in the range of 5 μF·cm^{-2}.[33] In consideration of the detected nonspecific binding for higher-generation dendritic wedges (G3), multiple injection cycles were further assessed to provide an insight into maximum packaging density for the SADMs. Six injection and purging cycles were evaluated for G3-SS-OH_{16}-sp as a model SADM surface. As can be seen in Figure 7, the first cycle provides a chain density of 0.38 molecule·nm^{-2} and a saturated level was obtained after four repetitive cycles with 16% increase, reaching a maximum attached amount of 0.44 molecule·nm^{-2}.

Hydroxyl- and Mannose-Functional SADMs for Attachment of *E. coli* MS7fim+ Cells. To evaluate the SADMs as potential biosensor surfaces, *E. coli* MS7fim+ cells were chosen as a model assay. These bacterial cells are involved in the uropathogenic colonization of bladder epithelium during urinary tract infections (UTIs). A critical part of this process is the bacterial cellular adhesion to mannosylated proteins at the surface of epithelial cells, facilitated by the FimH adhesive component located at the tips of type 1 pili.[45] One increasingly popular approach to novel therapeutics for UTIs has been to develop high-affinity antagonists for the bacterial lectin FimH,[46] where glycoconjugated dendrimers have shown great promise as multivalent scaffolds when applied in the bulk phase.[47−49] Consequently, four different fabricated SADM surfaces based on the extended spacer and a reference SAM decorated with

dx.doi.org/10.1021/la3041314 | *Langmuir* 2013, 29, 456−465

Table 3. Bioactive Mannose and Hydroxyl-Functional SADMs of Generations G1−G3 with Disulfide Cores[a]

name	SPR response (RU)	surface attachment ($ng \cdot cm^{-2}$)	chain density ($molecules \cdot nm^{-2}$)	funct group density ($OH \cdot nm^{-2}$)	*E. coli* binding (k $cells \cdot cm^{-2}$)	rel cell density (cells/pmol of end groups)
G1-SS-OH_4-sp	1263 ± 26	82.1 ± 1.7	1.37 ± 0.03	2.7 ± 0.06	357 ± 27	780
G3-SS-OH_{16}-sp	878 ± 308	57.1 ± 20.0	0.33 ± 0.1	3.0 ± 0.9	366 ± 49	850
G1-SS-Man_4-sp	1518 ± 297	98.7 ± 19.3	0.48 ± 0.09	0.95 ± 0.2	565 ± 39	3570
G3-SS-Man_{16}-sp	1951 ± 269	126.8 ± 17.5	0.17 ± 0.02	1.3 ± 0.2	919 ± 142	4170

[a]Measured by SPR in 70% EtOH.

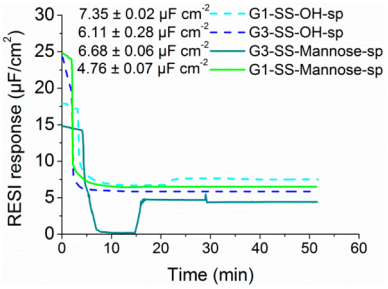

Figure 6. RESI response in 70% EtOH for G1 and G3 SADM gold surfaces functionalized with bioactive mannose and hydroxyl group.

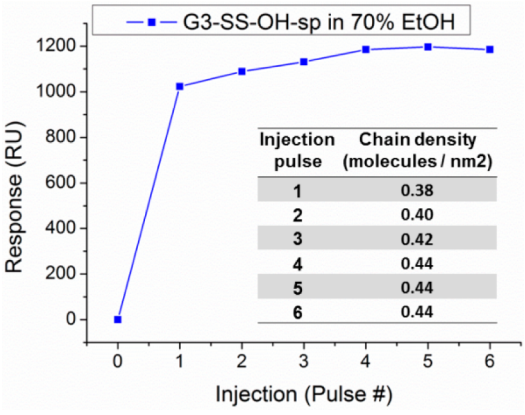

Figure 7. Multiple injections of G3-SS-OH-sp in 70% EtOH followed by purging cycles with AcB. Inset shows the amount of chains (per square nanometer) attached after each injection.

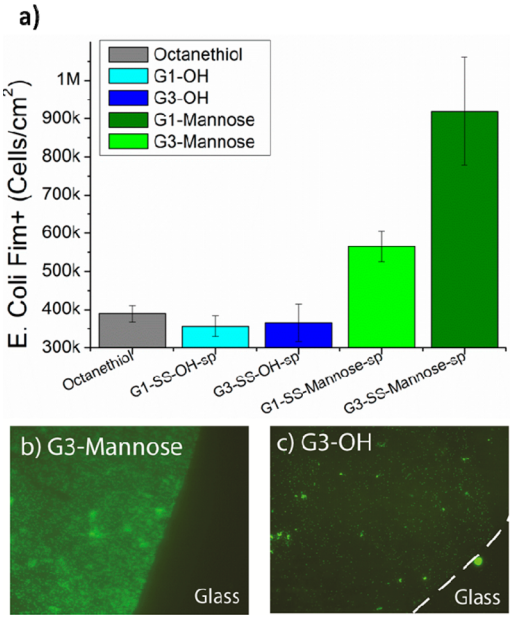

Figure 8. (a) Attachment of *E. coli* MS7fim+ cells on reference octanethiol and SADM sensor surfaces with bioactive mannose and hydroxyl functionality of generations G1 and G3. (b, c) Representative cell-covered sensor surfaces with (b) G3-SS-Man-sp and (c) G3-SS-OH-sp.

octanethiol molecules were used as biosensors to evaluate their interaction affinity toward *E. coli* MS7fim+ cells (Figure 8a). The sensor surfaces were incubated with *E. coli* MS7fim+ cells for 30 min under static conditions and purged with 300 mL of PBS buffer to exclude any poorly attached cells. For the hydroxyl-functional SADM surfaces, displaying the largest number of end groups (Figure 5b and Table 3), a low adsorption of *E. coli* MS7fim+ cells was found (ca. 800 cells/pmol of end groups). This nonspecific adhesion was similar to that of the octanethiol reference sensor. The highest density of adsorbed cells was acquired for the mannosylated sensor surface G3-SS-Man_{16}-sp , which displayed a superior solution scavenging capacity compared to both the hydroxyl-functionalized and G1-SS-Man_4-sp SADM surfaces. Normalizing the amount of cells bound per functional mannose group reveals a binding efficiency of approximately 4200 $cells \cdot (pmol\ of\ Man)^{-1}$ for the G3-SS-Man_{16} surface and 3600 $cells \cdot (pmol\ of\ Man)^{-1}$ for the G1-SS-Man_4-sp SADM surface (Figure 8). The overall cell scavenging ability for the G3 mannosylated surface corresponds to a 2.5-fold increase when compared to the G3 hydroxylated counterpart. As a result, mannosylated sensor surfaces based on SADMs increase the number of ligands and therefore display a superior bacterial binding capacity.

4. CONCLUSIONS

A library of aqueous soluble dendritic polyesters ranging from generation 1 to 3 and comprising sulfur groups enabled the spontaneous fabrication of self-assembled dendritic monolayers (SADMs) on gold surfaces. SADM surfaces were fabricated of different chain and functional group densities by altering the nature of the sulfur group, the dendritic wedge size, the distance between the sulfur group and the dendritic wedge, and the end group. SPR and RESI techniques revealed a rapid assembly upon injection and with excellent surface coverage in the range of well-insulated hydrophobic SAM layers. The gold surfaces were functionalized with dendritic wedges covering a density of 0.33−2.2 $molecules \cdot nm^{-2}$ and functional availability (hydroxyl or mannose) of 0.95−5.5 $groups \cdot nm^{-2}$. A direct cell recognition comparison between mannosylated and hydroxylated SADM surfaces revealed a 2.5-fold improvement in cell scavenging capacity for *E. coli* MS7fim+ bacteria. Finally, it is

dx.doi.org/10.1021/la3041314 | *Langmuir* 2013, 29, 456−465

apparent that SADMs based on polyester dendritic structure deliver a facile methodology to design well-defined bioactive gold sensor surfaces that yield improved cell-surface interactions.

■ ASSOCIATED CONTENT

Supporting Information

One scheme showing synthesis of 4-azidobutanoic acid, anhydride of succinic acid monoprop-2-ynyl ester, and azide-α-D-mannopyranoside **4**, and one figure showing the flow chamber for bacterial adhesion studies. This material is available free of charge via the Internet at http://pubs.acs.org.

■ AUTHOR INFORMATION

Corresponding Author

*E-mail Malkoch@kth.se (M.M.) or mattias.berglin@cmb.gu.se (M.B.).

Notes

The authors declare no competing financial interest.

■ ACKNOWLEDGMENTS

We acknowledge Vinnova-Sambio and the Swedish Research Council VR (2011-5358 and 2010-453) for financial support. Professor Malte Hermansson at the Department of Cell and Molecular Biology/Microbiology, Gothenburg University, is thanked for his assistance with *E. coli* cells.

■ REFERENCES

(1) Hawker, C. J.; Wooley, K. L. The convergence of synthetic organic and polymer chemistries. *Science* **2005**, *309*, 1200−1205.

(2) Mintzer, M. A.; Grinstaff, M. W. Biomedical applications of dendrimers: a tutorial. *Chem. Soc. Rev.* **2011**, *40*, 173−190.

(3) Percec, V.; Wilson, D. A.; Leowanawat, P.; Wilson, C. J.; Hughes, A. D.; Kaucher, M. S.; Hammer, D. A.; Levine, D. H.; Kim, A. J.; Bates, F. S.; Davis, K. P.; Lodge, T. P.; Klein, M. L.; De, V. R. H.; Aqad, E.; Rosen, B. M.; Argintaru, A. O.; Sienkowska, M. J.; Rissanen, K.; Nummelin, S.; Ropponen, J. Self-assembly of Janus dendrimers into uniform dendrimersomes and other complex architectures. *Science (Washington, DC, U. S.)* **2010**, *328*, 1009−1014.

(4) Gillies, E. R.; Frechet, J. M. J. Dendrimers and dendritic polymers in drug delivery. *Drug Discovery Today* **2005**, *10*, 35−43.

(5) Matthews, B. R.; Holand, G.: Antiviral dendrimers. U.S. Patent 6,190,650, 2001.

(6) Grinstaff, M. W. Dendritic macromers for hydrogel formation: Tailored materials for ophthalmic, orthopedic, and biotech applications. *J. Polym. Sci., Polym. Chem.* **2008**, *46*, 383−400.

(7) Mammen, M.; Choi, S. K.; Whitesides, G. M. Polyvalent interactions in biological systems: Implications for design and use of multivalent ligands and inhibitors. *Angew, Chem,. Int, Ed,* **1998**, *37*, 2755−2794.

(8) Roglin, L.; Lempens, E. H. M.; Meijer, E. W. A Synthetic "tour de force": Well-defined multivalent and multimodal dendritic structures for biomedical applications. *Angew. Chem., Int. Ed.* **2011**, *50*, 102−112.

(9) Han, H. J.; Kannan, R. M.; Wang, S.; Mao, G.; Kusanovic, J. P.; Romero, R. Multifunctional dendrimer-templated antibody presentation on biosensor surfaces for improved biomarker detection. *Adv. Funct. Mater.* **2010**, *20*, 409−421.

(10) Nakashima, T.; Satoh, N.; Albrecht, K.; Yamamoto, K. Interface modification on TiO_2 electrode using dendrimers in dye-sensitized solar cells. *Chem. Mater.* **2008**, *20*, 2538−2543.

(11) Malkoch, M.; Lundgren, A.; Hed, Y.; Oeberg, K.; Sellborn, A.; Fink, H.; Lowenhielm, P.; Kelly, J.; Berglin, M. Self-assembled arrays of dendrimer−gold−nanoparticle hybrids for functional cell studies. *Angew. Chem., Int. Ed.* **2011**, *50*, 3450−3453.

(12) Benhabbour, S. R.; Sheardown, H.; Adronov, A. Cell adhesion and proliferation on hydrophilic dendritically modified surfaces. *Biomaterials* **2008**, *29*, 4177−4186.

(13) Ostmark, E.; Macakova, L.; Auletta, T.; Malkoch, M.; Malmstrom, E.; Blomberg, E. Dendritic structures based on bis-(hydroxymethyl)propionic acid as platforms for surface reactions. *Langmuir* **2005**, *21*, 4512−4519.

(14) Friggeri, A.; Schonherr, H.; van Manen, H. J.; Huisman, B. H.; Vancso, G. J.; Huskens, J.; van Veggel, F.; Reinhoudt, D. N. Insertion of individual dendrimer molecules into self-assembled monolayers on gold: A mechanistic study. *Langmuir* **2000**, *16*, 7757−7763.

(15) Satoh, N.; Yamamoto, K. Self-assembled monolayers of metal-assembling dendron thiolate formed from dendrimers with a disulfide core. *Org. Lett.* **2009**, *11*, 1729−1732.

(16) Luscombe, C. K.; Proemmel, S.; Huck, W. T. S.; Holmes, A. B.; Fukushima, H. Synthesis of supercritical carbon dioxide soluble perfluorinated dendrons for surface modification. *J. Org. Chem.* **2007**, *72*, 5505−5513.

(17) Zhang, L.; Zou, B.; Dong, D.; Huo, F. W.; Zhang, X.; Chi, L. F.; Jiang, L. Self-assembled monolayers of new dendron-thiols: manipulation of the patterned surface and wetting properties. *Chem. Commun.* **2001**, 1906−1907.

(18) Zhang, L.; Huo, F. W.; Wang, Z. Q.; Wu, L. X.; Zhang, X.; Hoppener, S.; Chi, L. F.; Fuchs, H.; Zhao, J. W.; Niu, L.; Dong, S. J. Investigation into self-assembled monolayers of a polyether dendron thiol: Chemisorption, kinetics, and patterned surface. *Langmuir* **2000**, *16*, 3813−3817.

(19) Cho, T. J.; Zangmeister, R. A.; MacCuspie, R. I.; Patri, A. K.; Hackley, V. A. Newkome-type dendron-stabilized gold nanoparticles: Synthesis, reactivity, and stability. *Chem. Mater.* **2011**, *23*, 2665−2676.

(20) Bo, Z. S.; Zhang, L.; Zhao, B.; Zhang, X.; Shen, J. C.; Hoppener, S.; Chi, L. F.; Fuchs, H. Self-assembled monolayers of dendron-thiol on solid substrate. *Chem. Lett.* **1998**, 1197−1198.

(21) Gorman, C. B.; Miller, R. L.; Chen, K. Y.; Bishop, A. R.; Haasch, R. T.; Nuzzo, R. G. Semipermeable, chemisorbed adlayers of focally-substituted organothiol dendrons on gold. *Langmuir* **1998**, *14*, 3312−3319.

(22) Bain, C. D.; Troughton, E. B.; Tao, Y. T.; Evall, J.; Whitesides, G. M.; Nuzzo, R. G. Formation of monolayer films by the spontaneous assembly of organic thiols from solution onto gold. *J. Am. Chem. Soc.* **1989**, *111*, 321−35.

(23) Chechik, V.; Schoenherr, H.; Vancso, G. J.; Stirling, C. J. M. Self-assembled monolayers of branched thiols and disulfides on gold: Surface coverage, order and chain orientation. *Langmuir* **1998**, *14*, 3003−3010.

(24) Jiang, G. Q.; Deng, S. X.; Baba, A.; Huang, C. Y.; Advincula, R. C. On the monolayer adsorption of thiol-terminated dendritic oligothiophenes onto gold surfaces. *Macromol. Chem. Phys.* **2010**, *211*, 2562−2572.

(25) Lee, C. C.; Gillies, E. R.; Fox, M. E.; Guillaudeu, S. J.; Frechet, J. M. J.; Dy, E. E.; Szoka, F. C. A single dose of doxorubicin-functionalized bow-tie dendrimer cures mice bearing C-26 colon carcinomas. *Proc. Natl. Acad. Sci. U.S.A.* **2006**, *103*, 16649−16654.

(26) Wang, Q.; Mynar, J. L.; Yoshida, M.; Lee, E.; Lee, M.; Okuro, K.; Kinbara, K.; Aida, T. High-water-content mouldable hydrogels by mixing clay and a dendritic molecular binder. *Nature* **2010**, *463*, 339−343.

(27) Vestberg, R.; Malkoch, M.; Kade, M.; Wu, P.; Fokin, V. V.; Sharpless, K. B.; Drockenmuller, E.; Hawker, C. J. Role of architecture and molecular weight in the formation of tailor-made ultrathin multilayers using dendritic macromolecules and click chemistry. *J. Polym. Sci., Polym. Chem.* **2007**, *45*, 2835−2846.

(28) Montanez, M. I.; Hed, Y.; Utsel, S.; Ropponen, J.; Malmstrom, E.; Wagberg, L.; Hult, A.; Malkoch, M. Bifunctional dendronized cellulose surfaces as biosensors. *Biomacromolecules* **2011**, *12*, 2114−2125.

(29) Walter, M. V.; Lundberg, P.; Hult, A.; Malkoch, M. Novel macrothiols for the synthesis of a structurally comprehensive dendritic

library using thiol-ene click chemistry. *J. Polym. Sci., Part A: Polym. Chem.* **2011**, *49*, 2990−2995.
(30) Wilson, W. D. Analyzing biomolecular interactions. *Science* **2002**, *295*, 2103−2105.
(31) Voros, J. The density and refractive index of adsorbing protein layers. *Biophys. J.* **2004**, *87*, 553−561.
(32) Lundgren, A.; Hedlund, J.; Andersson, O.; Branden, M.; Kunze, A.; Elwing, H.; Hook, F. Resonance-mode electrochemical impedance measurements of silicon dioxide supported lipid bilayer formation and ion channel mediated charge transport. *Anal. Chem.* **2011**, *83*, 7800−7806.
(33) Hedlund, J.; Lundgren, A.; Lundgren, B.; Elwing, H. A new compact electrochemical method for analyzing complex protein films adsorbed on the surface of modified interdigitated gold electrodes. *Sens. Actuators, B* **2009**, *142*, 494−501.
(34) Krogfelt, K. A.; Bergmans, H.; Klemm, P. Direct evidence that the fimh protein is the mannose-specific adhesin of *Escherichia coli* type-1 fimbriae. *Infect. Immun.* **1990**, *58*, 1995−1998.
(35) McCormick, B. A.; Klemm, P.; Krogfelt, K. A.; Burghoff, R. L.; Pallesen, L.; Laux, D. C.; Cohen, P. S. *Escherichia coli* F-18 phase-locked on for expression of type-1 fimbriae is a poor colonizer of the streptomycin-treated mouse large-intestine. *Microb. Pathogen.* **1993**, *14*, 33−43.
(36) Bertani, G. Lysogeny at mid-twentieth century: P1, P2, and other experimental systems. *J. Bacteriol.* **2004**, *186*, 595−600.
(37) Wu, P.; Malkoch, M.; Hunt, J. N.; Vestberg, R.; Kaltgrad, E.; Finn, M. G.; Fokin, V. V.; Sharpless, K. B.; Hawker, C. J. Multivalent, bifunctional dendrimers prepared by click chemistry. *Chem. Commun.* **2005**, 5775−5777.
(38) Antoni, P.; Hed, Y.; Nordberg, A.; Nyström, D.; von Holst, H.; Hult, A.; Malkoch, M. Bifunctional dendrimers: From robust synthesis and accelerated one-pot postfunctionalization strategy to potential applications. *Angew. Chem., Int. Ed.* **2009**, *48*, 2126−2130.
(39) Polymer Factory Sweden AB: A provider of dendritic scaffolds based on the bis-MPA monomer. Available at http://www.polymerfactory.com.
(40) Kolb, H. C.; Finn, M. G.; Sharpless, K. B. Click chemistry: Diverse chemical function from a few good reactions. *Angew. Chem., Int. Ed.* **2001**, *40*, 2004−+.
(41) Ihre, H.; De Jesus, O. L. P.; Frechet, J. M. J. Fast and convenient divergent synthesis of aliphatic ester dendrimers by anhydride coupling. *J. Am. Chem. Soc.* **2001**, *123*, 5908−5917.
(42) Mrksich, M. A surface chemistry approach to studying cell adhesion. *Chem. Soc. Rev.* **2000**, *29*, 267−273.
(43) Biebuyck, H. A.; Bian, C. D.; Whitesides, G. M. Comparison of organic monolayers on polycrystalline gold spontaneously assembled from solutions containing dialkyl disulfides or alkenethiols. *Langmuir* **1994**, *10*, 1825−1831.
(44) Flink, S.; van Veggel, F. C. J. M.; Reinhoudt, D. N. Sensor functionalities in self-assembled monolayers. *Adv. Mater.* **2000**, *12*, 1315−1328.
(45) Chen, S. L.; Hung, C. S.; Pinkner, J. S.; Walker, J. N.; Cusumano, C. K.; Li, Z. L.; Bouckaert, J.; Gordon, J. I.; Hultgren, S. J. Positive selection identifies an in vivo role for FimH during urinary tract infection in addition to mannose binding. *Proc. Natl. Acad. Sci. U.S.A.* **2009**, *106*, 22439−22444.
(46) Han, Z. F.; Pinkner, J. S.; Ford, B.; Obermann, R.; Nolan, W.; Wildman, S. A.; Hobbs, D.; Ellenberger, T.; Cusumano, C. K.; Hultgren, S. J.; Janetka, J. W. Structure-based drug design and optimization of mannoside bacterial FimH antagonists. *J. Med. Chem.* **2010**, *53*, 4779−4792.
(47) Gouin, S. G.; Wellens, A.; Bouckaert, J.; Kovensky, J. Synthetic multimeric heptyl mannosides as potent antiadhesives of uropathogenic *Escherichia coli*. *ChemMedChem* **2009**, *4*, 749−755.
(48) Touaibia, M.; Wellens, A.; Shiao, T. C.; Wang, Q.; Sirois, S.; Bouckaert, J.; Roy, R. Mannosylated G(0) dendrimers with nanomolar affinities to *Escherichia coli* FimH. *ChemMedChem* **2007**, *2*, 1190−1201.
(49) Touaibia, M.; Roy, R. Glycodendrimers as anti-adhesion drugs against type 1 fimbriated *E. coli* uropathogenic infections. *Mini-Rev. Med. Chem.* **2007**, *7*, 1270−1283.